n-ZnO/$LaAlO_3$/p-Si heterojunction for visible-blind UV detection

D. S. Tasi,[1] C. F. Kang,[1] H. H. Wang,[1] C. A. Lin,[1] J. J. Ke,[1] Y. H. Chu,[2] and J. H. He[1,*]

[1]*Institute of Photonics and Optoelectronics and Department of Electrical Engineering, National Taiwan University, Taipei 10617, Taiwan*

[2]*Department of Materials Science and Engineering, National Chiao Tung University, Hsinchu 30010, Taiwan*

**Corresponding author: jhhe@cc.ee.ntu.edu.tw*

Received November 16, 2011; revised January 28, 2012; accepted January 29, 2012; posted January 30, 2012 (Doc. ID 158336); published March 15, 2012

A visible-blind UV photodetector (PD) using a double heterojunction of n-ZnO/$LaAlO_3$ (LAO)/p-Si was demonstrated. Inserted LAO layers exhibit electrical insulating properties and serve as blocking layers for photoexcited electrons from p-Si to n-ZnO, leading to an enhanced rectification ratio and a visible-blind UV detectivity of the n-ZnO/LAO/p-Si PDs due to the high potential barrier between LAO and p-Si layers (~2.0 eV). These results support the use of n-ZnO/LAO/p-Si PDs in the visible-blind UV PDs in a visible-light environment.

OCIS codes: 040.7190, 230.5160, 250.0040.

Visible-blind UV photodetectors (PDs) have drawn intense interest in combustion flame monitoring, pollution analysis, missile plume detection, chemical sensing, and intersatellite communications [1–4]. ZnO is an excellent semiconductor material for UV detection due to its wide bandgap [5–7]. Previous reports have demonstrated a variety of ZnO-based PDs, including photoconductors [6], metal–semiconductor–metal PDs [8], Schottky photodiodes [4,9], and p-n photodiodes [8,10–12]. ZnO-based Schottky PDs can serve as UV PDs only because of the wide bandgap (3.3 eV) of ZnO and have relatively high reverse leakage current. Moreover, the increase in reverse leakage current with temperature leads to a thermal instability issue in ZnO-based Schottky PDs [13]. A p-n PD has the advantages of fast response and low dark current and the ability to work without applied bias. However, due to the lack of reliable p-type ZnO, the heterojunctions used for ZnO-based UV photodiodes are of a different p-type material [8,11]. Low-cost p-Si is a candidate for the n-ZnO-based heterojunction UV detector due to its compatible processing with a complementary metal–oxide–semiconductor [10–12]. Many studies on n-ZnO/p-Si heterojunction photodiodes have been done [8,10–12,14]. However, while the n-ZnO/p-Si photodiode does enhance UV responses due to ZnO, it still has a significant response to visible light, which greatly hinders its applications in UV detection, particularly in a visible-light environment.

In this work, we present the UV PDs employing n-ZnO/$LaAlO_3$ (LAO)/p-Si double heterojunctions using pulse laser deposition (PLD). The n-ZnO/LAO/p-Si PDs exhibit visible-blind UV responsivity with a cutoff wavelength of responsivity at 380 nm, corresponding to the near band edge (NBE) absorption of ZnO [15,16]. Inserted LAO layers 10 nm thick effectively eliminate visible-light responses via blocking the electrons excited by visible photons in p-Si near the interface owing to the high potential barrier between the p-Si and LAO layers (~2.0 eV). This study paves the way for visible-blind UV photosensing applications under outdoor lighting.

Figure 1(a) shows the schematic of the n-ZnO/LAO/p-Si PDs. The 10 nm thick LAO and 100 nm thick n-ZnO thin films were deposited on p-Si using a PLD system. Before being loaded into the growth chamber, p-Si wafers were cleaned for 1.5 min in the buffered oxide etchant to remove the surface native oxide layer. A KrF excimer laser (wavelength: 248 nm, laser energy: 1.3 J/cm^2, and repetition rate: 10 Hz) was applied to ablate the targets of pure LAO and ZnO. The temperature of the substrate holder was ~700 °C, and the partial pressure of oxygen was 0.1 Torr (the base pressure of the PLD chamber was 1×10^{-6} Torr). The PDs were defined using photolithography with active areas of 500 μm × 158 μm contacted by interdigitated Au/Ti electrodes with an 8 μm wide, 150 μm long, and 50 nm thick, with spacing 8 μm wide on the n-ZnO/LAO/p-Si PD. The 30 nm thick Au/Ni electrodes were made on the backside of p-Si. In order to highlight the visible-blind UV response of n-ZnO/LAO/p-Si PDs, n-ZnO/p-Si PDs without LAO

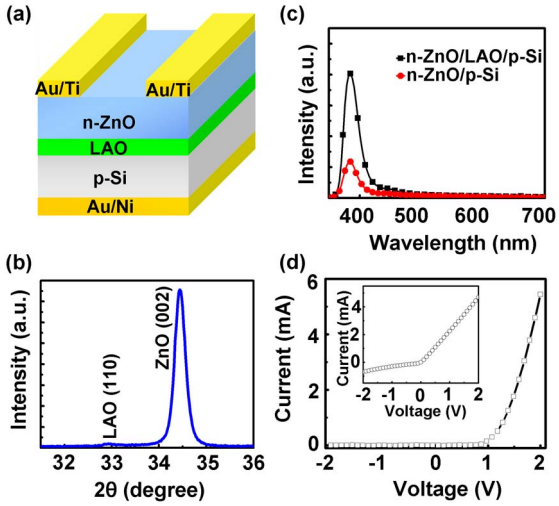

Fig. 1. (Color online) (a) Schematic of the n-ZnO/LAO/p-Si PDs, (b) x-ray diffraction spectrum of n-ZnO/LAO/p-Si layers, (c) room-temperature photoluminescence spectra of n-ZnO/LAO/p-Si and n-ZnO/p-Si layers, and (d) *I-V* curve of n-ZnO/LAO/p-Si PDs in the dark. The inset in (d) is the *I-V* curve of n-ZnO/p-Si PDs in the dark.

layers were fabricated with identical processes as a reference.

After the PLD growth processes, the x-ray diffraction (XRD) spectrum of n-ZnO/LAO/p-Si was measured with a fixed incident angle of 0.5 deg for the phase identification, as shown in Fig. 1(b). A strong peak is at 34.52 deg for the diffraction from the (002) plane of ZnO, showing that ZnO films are preferentially oriented in the *c*-axis direction [17]. A weak and broad peak from the (110) plane of LAO is observed in the XRD spectrum, indicating the LAO layer with a nanocrystalline (i.e., amorphous) structure. To further confirm the quality of ZnO films, the room-temperature photoluminescence (PL) spectra of n-ZnO/LAO/p-Si and n-ZnO/p-Si were measured with a 325 nm He–Cd laser as an excitation source, as shown in Fig. 1(c). The PL spectra of ZnO show a strong NBE emission at 380 nm and no defect band emission in visible regions [15], indicating the superior crystal quality of the ZnO thin films grown by the PLD method compared with ZnO nanorods grown by the hydrothermal method [16]. Moreover, the FWHMs of NBE peaks of n-ZnO/LAO/p-Si and n-ZnO/p-Si are 20 and 22 nm, respectively, indicating that LAO layers are suitable buffers to reduce the lattice mismatch between n-ZnO layers and p-Si substrates. It should be noted that the lattice mismatches of ZnO/Si, ZnO/LAO, and LAO/Si are ~40%, 3%–5%, and ~1.3%, respectively [18–20]. Figure 1(d) shows the *I-V* curve of n-ZnO/LAO/p-Si PDs measured with a Keithley 4200-SCS semiconductor characterization system in the dark. The n-ZnO/LAO/p-Si PD exhibits the low reverse dark current (~1 μA) under −2 V bias and a rectification ratio of $\sim 10^3$ at ±2 V, indicating the electrical insulating nature of the LAO layers with thicknesses as low as 10 nm. In contrast, as shown in the inset of Fig. 1(d), a rectification ratio of n-ZnO/p-Si PDs without LAO layers is ~10 at ±2 V due to the high reverse dark current (~0.4 mA) under the bias of −2 V.

Figure 2 shows the spectral responsivity of the n-ZnO/LAO/p-Si PDs measured with the EQE-R3011 spectral response system (Enli Technology) under different biases. The visible-light response of n-ZnO/LAO/p-Si PDs is diminished as the reverse bias is decreased. As shown in the inset of the external quantum efficiency (EQE) spectrum in Fig. 2, the n-ZnO/LAO/p-Si PDs at 0.5 V reverse bias show high UV response (the responsivity and EQE at 350 nm are ~0.05 A/W and ~18%, respectively), with a sharp cutoff at 380 nm and obscure visible-light response, demonstrating visible-blind UV detection. The n-ZnO/LAO/p-Si PDs under a reverse bias higher than 0.5 V show notable visible-light signals and significant UV responses due to the NBE absorptions of Si and ZnO, respectively, as shown in Fig. 2. The reverse-bias-insensitive UV response of n-ZnO/LAO/p-Si PDs is due mainly to the full depletion of n-ZnO layers. It should be noted that the 100 nm thick n-ZnO thin films stay fully depleted at a reverse bias higher than 0.5 V. Since UV photocarrier generation occurs at a boundary between ZnO and LAO, we can treat Si as a conductive electrode. Considering the thin LAO insulator layers, the depletion width of n-ZnO adjacent to the oxide–semiconductor interface can be approximated as $W_n = (2\varepsilon V_r/eN_D)^{1/2}$, where W_n is the depletion width of n-ZnO, V_r is the reverse-bias voltage, ε is the dielectric constant of n-ZnO ($12 \times 8.85 \times 10^{-14}$ F/cm); and N_D is the donor concentration of n-ZnO, $\sim 5 \times 10^{16}$ cm^{-3} [21–23].

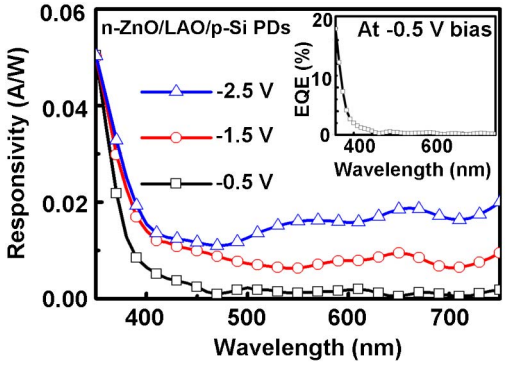

Fig. 2. (Color online) Spectral responsivity of the n-ZnO/LAO/p-Si PDs under reverse biases of 0.5, 1.5, and 2.5 V. The inset is the external quantum efficiency of the n-ZnO/LAO/p-Si PDs at −0.5 V bias from 350 to 750 nm.

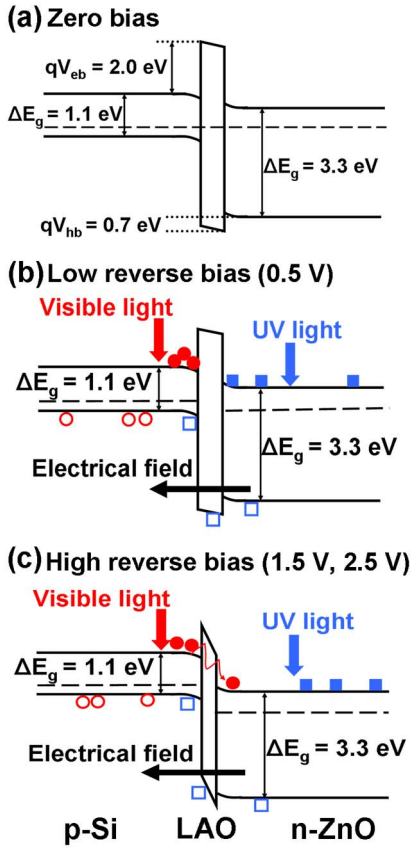

Fig. 3. (Color online) The band structure of n-ZnO/LAO/p-Si at (a) zero bias in the dark, (b) low reverse bias (0.5 V) under illumination, and (c) high reverse bias (1.5 and 2.5 V) under illumination. Solid circles and open circles are the electrons and the holes, respectively, photoexcited in the depletion region of p-Si by visible light; solid squares and open squares are the electrons and holes, respectively, photoexcited in the depletion region of n-ZnO by UV light spectral responsivity curves of the n-ZnO/LAO/p-Si PDs under reverse biases of 0.5, 1.5, and 2.5 V. Note that the potential barrier for electrons (V_{eb}) in p-Si at the p-Si–LAO interface and the potential barrier for holes (V_{hb}) in n-ZnO at the LAO–n-ZnO interface are ~2.0 eV and ~0.7 eV, respectively.

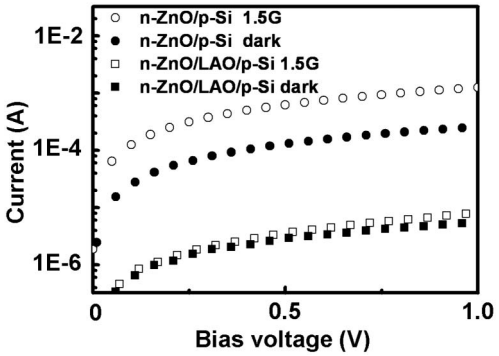

Fig. 4. $I-V$ curves of the n-ZnO/LAO/p-Si and n-ZnO/p-Si PDs measured in the dark and under air mass 1.5 global illumination.

Accordingly, W_n is estimated to be ~115 nm under a reverse bias of 0.5 V.

To gain insight into the physics behind the visible-blind UV response of n-ZnO/LAO/p-Si PDs, the band structure of n-ZnO/LAO/p-Si from the Anderson model is illustrated in Fig. 3 [11,24]. At zero bias, the band structure of the n-ZnO/LAO/p-Si heterojunction at thermal equilibrium is shown in Fig. 3(a). The potential barrier for electrons in p-Si at the p-Si—LAO interface and the potential barrier for holes in n-ZnO at the LAO–n-ZnO interface are ~2.0 eV and ~0.7 eV, respectively. As shown in Fig. 3(b), at low reverse bias (0.5 V), the electron–hole pairs excited by photons with wavelengths longer than 380 m penetrating through ZnO layers to the depletion regions of the p-Si are swept out immediately by the internal electric field, but the photoexcited electrons in the p-Si are blocked at the interface between p-Si and LAO layers due to the high potential barrier (~2.0 eV) and thus recombine with the holes quickly, reducing the photocurrent in visible wavelength regions. On the other hand, the electro–hole pairs excited by photons with wavelengths shorter than 380 nm within the depletion regions of the n-ZnO layer can be separated effectively, and then photoexcited holes can penetrate easily through the LAO layer to p-Si because of low barrier potential (~0.7 eV), giving rise to high photocurrents in UV wavelength regions. Here p-Si serves as a conductive layer for UV photoexcited holes. Therefore, the visible-blind UV response of n-ZnO/LAO/p-Si PDs is achieved by restraining visible-light response under low reverse bias. One should note that, as shown in Fig. 3(c), at a high reverse bias, such as 1.5 or 2.5 V, the excess electrons excited by visible light in p-Si can tunnel through thin LAO layers under a high electrical field, resulting in significant photoresponses in visible wavelength regions, as shown in Fig. 2.

In order to highlight the visible-blind UV response of n-ZnO/LAO/p-Si PDs, n-ZnO/p-Si PDs were fabricated as a comparison. Figure 4 shows the I-V characteristics of the n-ZnO/LAO/p-Si and n-ZnO/p-Si PDs measured in the dark and under air mass (AM) 1.5 global (G) illumination. Under 0.5 V of the reverse bias, the photocurrent to dark current ratios (PDCRs) of n-ZnO/LAO/p-Si PDs and n-ZnO/p-Si PDs are 0.2 and 4.5, respectively, using $\mathrm{PDCR} = (I_p - I_d)/I_d$, where I_d is the dark current and I_p is the photocurrent under AM 1.5 G illumination [16,25]. Note that the integrated UV (<400 nm) and visible (400–700 nm)-light power in AM 1.5 G are ~3% and ~45%, respectively. Accordingly, the low PDCR of n-ZnO/LAO/p-Si PDs under AM 1.5 G illumination is due to the fact that inserted LAO layers effectively restrain visible-light responses.

In summary, n-ZnO/LAO/p-Si exhibits a rectification ratio of $\sim 10^3$ at ±2 V, while the rectification ratio is low for conventional n-ZnO/p-Si PDs (~10 at ±2 V). The LAO layers exhibit electrical insulating characteristics and serve as blocking layers for photoexcited electrons from p-Si to n-ZnO, leading to a high rectification ratio and visible-blind UV detectivity of n-ZnO/LAO/p-Si PDs. This work demonstrates that the LAO layers incorporated with n-ZnO and p-Si hold promise for visible-blind UV detection.

References

1. E. Monroy, F. Omnes, and F. Calle, Semicond. Sci. Technol. **18**, R33 (2003).
2. C. Soci, A. Zhang, B. Xiang, S. A. Dayeh, D. P. R. Aplin, J. Park, X. Y. Bao, Y. H. Lo, and D. L. Wang, Nano Lett. **7**, 1003 (2007).
3. J. H. He, P. H. Chang, C. Y. Chen, and K. T. Tsai, Nanotechnology **20**, 135701 (2009).
4. Q. Yang, X. Guo, W. Wang, Y. Zhang, S. Xu, D. H. Lien, and Z. L. Wang, ACS Nano **4**, 6285 (2010).
5. T. Zhai, X. Fang, M. Liao, X. Xu, H. Zeng, B. Yoshio, and D. Golberg, Sensors **9**, 6504 (2009).
6. C. Soci, A. Zhang, X. Bao, H. Kim, Y. Lo, and D. L. Wang, J. Nanosci. Nanotechnol. **10**, 1430 (2010).
7. J. G. Lu, P. C. Chang, and Z. Fan, Mater. Sci. Eng. R.: Reports **52**, 49 (2006).
8. K. Liu, M. Sakurai, and M. Aono, Sensors **10**, 8604 (2010).
9. J. Zhou, Y. D. Gu, Y. F. Hu, W. J. Mai, P. H. Yeh, G. Bao, A. K. Sood, D. L. Polla, and Z. L. Wang, Appl. Phys. Lett. **94**, 191103 (2009).
10. S. Mridha and D. Basak, J. Appl. Phys. **101**, 083102 (2007).
11. J. H. He and C. H. Ho, Appl. Phys. Lett. **91**, 233105 (2007).
12. I. S. Jeng, J. H. Kim, and S. Im, Appl. Phys. Lett. **83**, 2946 (2003).
13. H. V. Wenckstern, S. Muller, G. Biehne, H. Hochmuth, M. Lorenz, and M. Grundmann, J. Electron. Mater. **39**, 559 (2010).
14. K. Sun, Y. Jing, N. Park, C. Li, Y. Bando, and D. L. Wang, J. Am. Chem. Soc. **132**, 15465 (2010).
15. C. A. Lin, D. S. Tsai, C. Y. Chen, and J. H. He, Nanoscale **3**, 1195 (2011).
16. D. S. Tsai, C. A. Lin, W. C. Lien, H. C. Chang, Y. L. Wang, and J. H. He, ACS Nano **5**, 7748 (2011).
17. X. D. Wang, J. Song, P. Li, J. H. Ryou, R. D. Dupuis, C. J. Summers, and Z. L. Wang, J. Am. Chem. Soc. **127**, 7920 (2005).
18. B. E. Park and H. Ishiwara, Appl. Phys. Lett. **82**, 1197 (2003).
19. J. S. Tian, M. H. Liang, Y. T. Ho, Y. A. Liu, and L. Chang, J. Cryst. Growth **310**, 777 (2008).
20. S. Xu and Z. L. Wang, Nano Res. **4**, 1013 (2011).
21. S. M. Sze and K. K. Ng, *Physics of Semiconductor Devices* (Wiley, 2007), pp. 126–127.
22. Y. F. Gu, X. M. Li, J. L. Zhao, W. D. Yu, X. D. Gao, and C. Yang, Solid State Commun. **143**, 421 (2007).
23. H. Lin and C. W. Liu, Sensors **10**, 8797 (2010).
24. L. F. Edge, D. G. Schlom, S. A. Chambers, E. Cicerrella, J. L. Freeouf, B. Holländer, and J. Schubert, Appl. Phys. Lett. **84**, 726 (2004).
25. W. C. Lien, D. S. Tsai, S. H. Chiu, D. G. Senesky, R. Maboudian, A. P. Pisano, and J. H. He, IEEE Electron Device Lett. **32**, 1564 (2011).